Fabrication and Powering Test of a High-Temperature Superconducting Periodic Quadrupole Driving a Short-Length Transport Line for Laser-Plasma Accelerators

S. Fatehi, A. Bernhard, S. C. Richter, A. Grau, M. Eisele, F. Hornung, T. Arndt, and A.-S. Müller

***Abstract*—Laser-plasma accelerators, have extremely high accelerating gradients and can generate ultra-short electron bunches with micrometer bunch lengths which makes them a prominent candidate to drive the next-generation compact light sources and free-electron lasers (FELs). To fully exploit the advantages of this novel accelerating technology and to compensate for large chromatic effects in the beam transport line, novel compact beam optic elements based on high-temperature superconductor technology are studied. Moreover, the limited mechanical properties of the HTS ceramic-structured superconductors lead to many manufacturing issues during the coil winding process and to ease this difficulty, designing magnets with simple shape coils is of interest. In this article, the magnet design as well as the fabrication and test of a demonstrator of a periodic iron-core miniature HTS quadrupole is discussed. This magnet features simple pancake coils that are capable of providing high field gradients and in the experiments were successfully powered in liquid nitrogen and liquid helium showing no degradation.**

***Index Terms*—Accelerator magnets, HTS coils, magnet design and analysis techniques, no-insulation coils.**

I. Introduction

LASER-PLASMA Acceleration (LPA) is a promising method for accelerating electrons in a few cm length to GeV energies using ionized plasma and high-power lasers. LPAs have the advantage of compact size and potential applications in radiation sources and free-electron lasers [1], [2], [3]. However, the energy spread and divergence of the accelerated beams are major challenges that need to be overcome. To address these challenges, an effective beam transport line is necessary, along with a radiation source that accepts the dispersed electron beam and generates monochromatic radiation like a transverse gradient undulator (TGU) [4]. In recent years, different transport lines at varying energies from 120 MeV to 700 MeV have been designed and developed at KIT, employing normal conducting and high-temperature superconducting (HTS) magnets, [5], [6], [7]. To develop reliable lab-scaled transport lines at high energy levels, different magnet designs using HTS technology were explored [8]. However, the mechanical limitations of HTS ceramic-structured superconductors can cause strain and stress in the material, leading to performance degradation. To overcome the manufacturing issues in coil winding with HTS superconductors, a novel periodic magnet with simple pancake-shaped coils was designed and developed that not only simplifies the winding process but is also capable of providing sufficiently high field gradients to enable highly compact beam transport lines as shown in Fig. 1. The magnet design and beam optics calculations for a 1.4 m transport line using HTS periodic iron-core magnets are discussed in detail in [9]. In this contribution, the fabrication and powering test results of half a period of the HTS periodic quadrupole are presented.

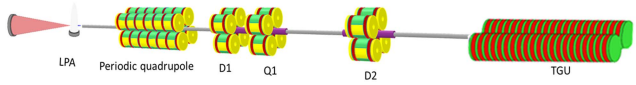

Fig. 1. Schematics of the HTS iron-core transport line using HTS periodic magnets.

II. Periodic Quadrupole Design

The periodic quadrupole configuration utilizes a set of HTS pancake coils, with an inner radius of 21 mm and an outer radius of 25 mm, which are situated on a cylindrical iron yoke in a way that the neighboring coils have opposite directions of current. This arrangement forms a periodic structure with period length λ. The iron yoke is designed with optimized hyperbolic iron poles, in order to create the desired quadrupolar field shape with a good field quality, i.e. in the order of 10^{-4}, within the magnet gap. Using CST and Opera simulation codes [10], [11], which are fully featured software packages include FEM solvers dedicated to static and transient applications, the 3D design of the magnet was explored to determine the number of periods and the periodic length required for the beam capture. The magnet design was done in parallel to the beam dynamics simulation with the code ASTRA [12], in order to ensure an efficient capture

This work was supported by the BMBF project 05K19VKA PlasmaFEL (Federal Ministry of Education and Research). *(Corresponding author: S. Fatehi.)*

The authors are with the Karlsruhe Institute of Technology (KIT), 76131 Karlsruhe, Germany (e-mail: Samira.Fatehi@kit.edu).

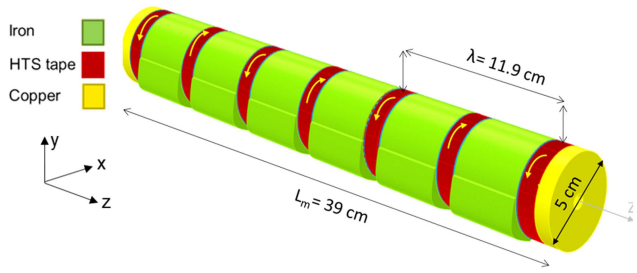

Fig. 2. One-fourth of the optimized HTS iron-core periodic quadrupole.

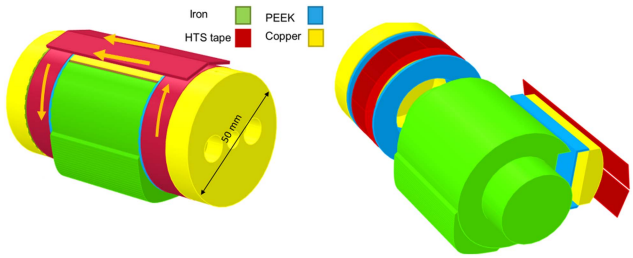

Fig. 3. Half a period model designed with Opera 3D, general view with current direction (left) and detailed view (right).

TABLE I
COIL SPECIFICATIONS FOR THE PERIODIC QUADRUPOLE MAGNET

Parameter	**Unit**	**Value at** 4.2 K	**Value at** 77 K
Coil cross-section	mm^2	12.00 × 4.00	
No. turns	-	72.00	
Current per turn	A	1330.00	135.72
Current density	$A\,mm^{-2}$	2000.00	203.58
Field at conductor	T	6	0.65

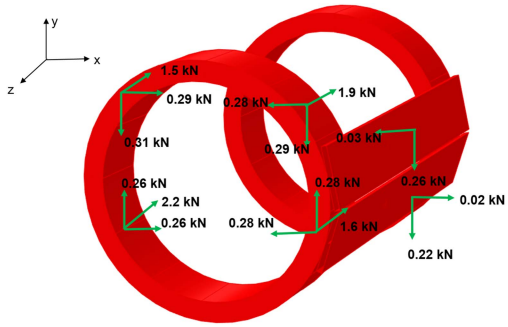

Fig. 4. Lorentz forces on HTS bridge and coils at 4.2 K.

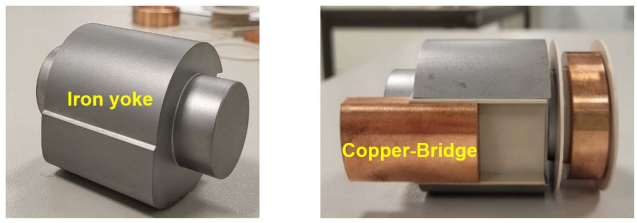

Fig. 5. Winding body demonstrator.

and transportation of the LPA-generated bunches in this periodic magnet structure. An iterative process determined that a 3-period model with a periodic length $\lambda = 11.9\,\text{cm}$ yields an efficient electron beam focusing in both transverse planes.

Fig. 2 shows the optimized magnet structure which comprises coils wound with 12 mm wide SCS12030-AP ReBCO tape from Superpower Inc. [13], with each coil consisting of 72 turns. The magnet can generate a maximum field gradient of $170\,\text{T}/\text{m}$ with a current of 1.3 kA when operated at 4.2 K. The coils are connected by two HTS tapes on the back yoke, and the simulation demonstrates that the currents in the HTS bridges counteract each other throughout the entire magnet structure. Consequently, bridge currents have no notable effect on the field or field quality along the beam path. Detailed specifications of the coils are summarized in Table I.

III. DEMONSTRATOR FABRICATION

Prototyping half a period of the periodic quadrupole was realized in-house. To protect the magnet from high current densities, non-insulated (NI) ReBCO tapes (see [14]) were wound on oxygen-free copper parts. This design allows the current to bypass local normal conducting zones and in this way protect the coils from damage e.g. during a quench event. The key idea behind using NI coils is to eliminate turn-to-turn insulation in the pancake coil, enabling current to naturally bypass hot spots through turn-to-turn contacts. To maintain the current within the coil and copper bodies, ground electrical insulation is used. As depicted in Fig. 3, the iron yoke is insulated from the coils and the copper parts using PEEK (Poly-Ether Ether Ketone) insulators which are high-performance thermoplastic polymers known for their high mechanical strength over a wide temperature range and can serve as an alternative to G10/G11 in superconducting applications. To check the mechanical layout of the demonstrator before fabrication and coil winding, the forces were investigated on the coils as well as on the HTS bridge tapes using the Opera magneto-static solver. The calculations were performed at a temperature of 4.2 K using the parameters listed in Table I and the resulting forces on the HTS coils and tapes are illustrated in Fig. 4. The forces are displayed for the left-hand side coil, however, owing to symmetry, identical forces are applied to the right-hand side coil. Looking at each coil individually, there is no inherent symmetry, especially considering the back part that is soldered to the HTS bridges. The investigation revealed that the maximum force acting on the coils is in the longitudinal direction (z), amounting to a total of 7.7 kN on each coil. However, this longitudinal force is effectively counteracted in the model by the presence of the iron yoke and the two copper ends. The transverse forces (F_x and F_y) on the HTS bridges, with $F_x = 0.02$ kN on the lower tape and a maximum value of $F_y = 0.26$ kN on the upper tape. Nevertheless, to ensure additional stability, these forces were mechanically treated by fastening the HTS bridge tapes to the copper bridge from the upper side using Kapton tape. Also, it is planned to add a copper part on top of the bridges in the upgrade of the demonstrator which would provide more resistance against any potential transverse forces. Fig. 5 shows the winding body fabricated in-house. The iron yoke in the front view includes the quadrupole pole profile which shapes the field lines and the back view includes the copper bridge placed on the PEEK insulator.

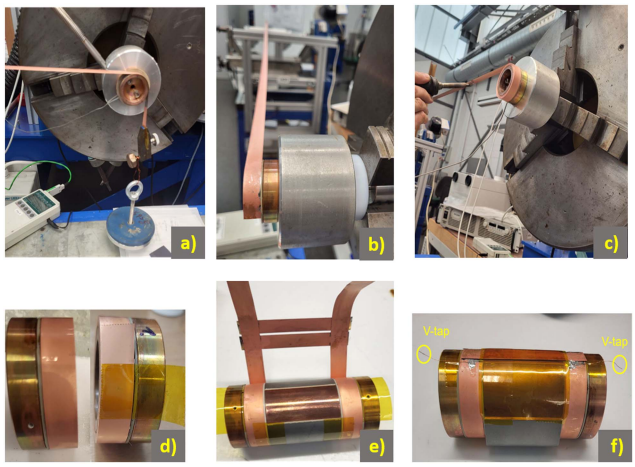

Fig. 6. (a) Soldering the first turn of ReBCO tape on the copper body. (b) Winding of the 72 turns. (c) Last turn soldering. (d) Wound pancake coils. (e) Soldered HTS bridge tapes. (f) Magnet demonstrator.

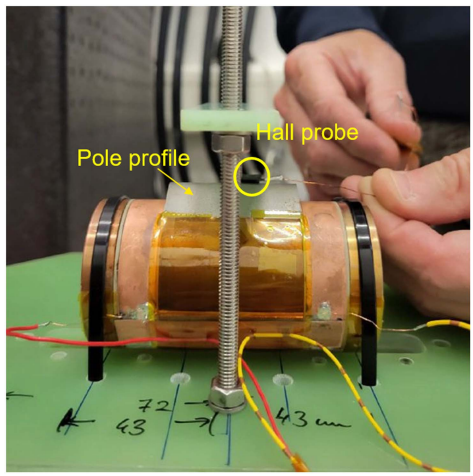

Fig. 7. Field measurement setup.

IV. Coil Winding

The HTS coils were wound with a 12 mm wide SCS12030-AP ReBCO tape on the copper winding bodies with the superconducting layer faced up, i.e. the substrate side lays on the copper body. Soldering was used to fix the HTS coils to the copper bodies and establish electrical connections between the HTS coils and the HTS tapes on the bridge. The inner turn of the HTS-coated conductor for each coil was soldered to the copper body using Sn60Pb40 solder wire and a heating structure which was placed beside the copper body, on the winding machine. The temperature for soldering the first turn was up to 230 °C for 10 minutes.

After soldering the first turn to the copper body, the winding was continued for 72 turns with 25 N winding tension, and the outer turn soldering was performed using an indium-based low-temperature soldering wire Sn50In50. In this step, the middle part of the last turn was soldered to the penultimate turn by heating up the whole coil to the melting point of Sn50In50 which is 118 °C. During the heating process, the temperature on the tapes was kept below 200 °C to protect the first-turn soldering and the HTS tape. Using the described procedure both coils were wound successfully. In the final phase of winding the coils, the two coils were connected by soldering the end turn of each coil to the two HTS bridge tapes. To achieve minimal joint resistance on the soldering surface, the bridges and the last turns of the coils were soldered face-to-face with their ReBCO layers, using a heating plate. After completing the soldering of the coils to the bridges on the heating plate, an iron weight was placed on top of the bridge to apply pressure and then the heating plate was turned off to allow the entire system to cool down. Also, two copper wires were placed on each coil as voltage taps (V-taps) to measure the voltage over different parts of the coil assembly during the powering test. Fig. 6 shows the winding process as well as the two wound pancake coils assembled with the iron yoke.

V. Powering of the Coils and Experimental Results

To evaluate the function of the coils in generating the required magnetic field, magnetic measurement tests were performed. Since the demonstrator is one-fourth of a quadrupole, a valid measurement was to measure the pole tip field at the longitudinal center of the quadrupole, i.e., at $z = 0$. To do the magnetic measurement the following setup was arranged: as it is shown in Fig. 7, the demonstrator was fixed on a G10 plate at the two ends, by wrapping two fixing bands on the copper ends. On the central plane of the magnet, two screwed rods were placed on the two sides in which a small rectangular G10 plate could be moved up and down above the pole profile. A Hall probe was glued at the center of this plate which, by moving the plate down to the pole profile, could measure the field on the pole tip. Also, it was important to have an estimate of the critical current before powering the coils. So, the HTS critical current database for a 12 mm wide single tape from the website of the Victoria University of Wellington [15] was extracted and intersected with the load line derived from Opera simulations. That gives an estimate of the critical current around 135 A, as detailed in [8].

A. Liquid Nitrogen Measurements

To start powering the coils, the whole setup was cooled down to 77 K in a liquid nitrogen bath and the coils were powered to 150 A, using a current ramping rate of 10 A/min. Throughout the experiment, critical current values in both coils were identified when the voltage exhibited a non-linear increase during the current ramp-up. Fig. 8 shows that the voltage over each coil demonstrated a linear dependence on the current up to 125 A for coil I and 122 A for coil II which are both less than the theoretically calculated critical current 135 A, as expected. This consistent slope indicates the resistances of the normal conducting parts, encompassing copper bodies, wirings, and joint resistances, as depicted schematically in Fig. 9. The total resistances for both coils were of the order of a few μΩ at 77 K, specifically 2.4 μΩ for coil I and 8.1 μΩ for coil II. Furthermore, coil II reaches its critical current a few amperes sooner than coil I, that is 122 A which can be due to the different contact resistances between tapes in coil II with respect to the coil I comes from unwanted inaccuracy during the winding process. Moreover, by correcting the results to the normal conducting

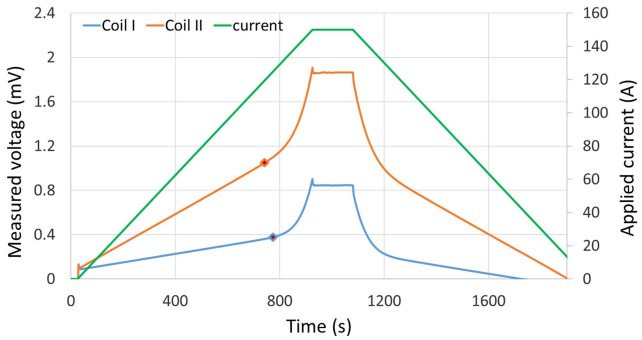

Fig. 8. Measured voltage and current over coil I and coil II versus time at 77 K, dots represent the critical points.

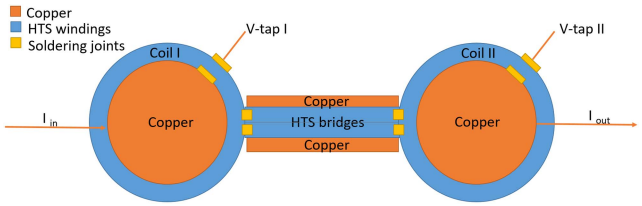

Fig. 9. Schematic of the winding structure showing HTS and normal conducting parts; current leads (I_{in} and I_{out}), voltage measurement wiring on the coils (V-taps), soldering joints, and copper bodies.

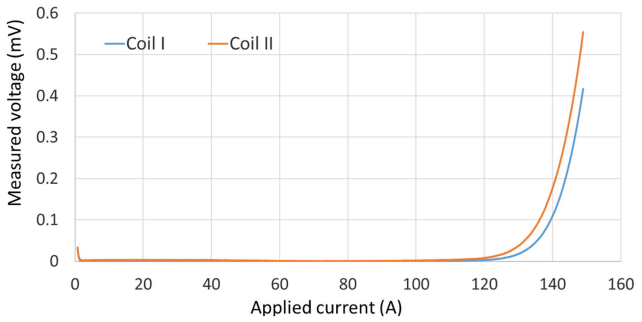

Fig. 10. Measured voltage over coil I and coil II versus current at 77 K, values are corrected to the normal conducting parts' resistances.

parts' resistances, the measured voltage over coil I and coil II versus current is obtained as depicted in Fig. 10. By ramping up to the critical current values 125 A and 122 A, there is approximately zero resistance for the two coils, and if the current is further increased a resistance appears. In fact, by increasing the current, each turn reaches its critical current I_c, and by filling up the turns the current flows radially within the non-insulated turns. In this powering test, despite having the radially flowing currents for current values higher than I_c, the coils were powered successfully up to 120% of the critical current, i.e., 150 A. After ceasing the current ramping, due to the non-insulated tape turns, the current needs time to re-distribute and there would be a current/voltage decay, as can be seen in Fig. 8 at the $t = 926$ s.

B. Liquid Helium Measurements

Powering and magnetic measurements at LHe temperature were done in the CASPER I cryostat at 4.2 K at KIT [16], using

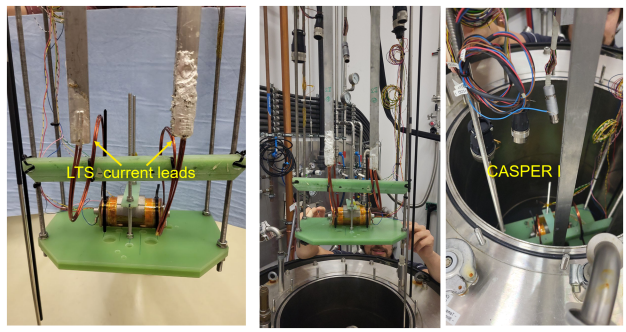

Fig. 11. Measurement setup in CASPER I at liquid helium temperature.

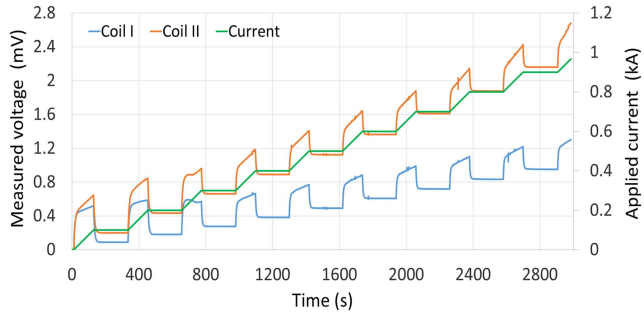

Fig. 12. Measured voltage and current over coil I and coil II versus time at 4.2 K.

two LTS current leads and the aforementioned setup, Fig. 11. For this, the coils were powered up with a current ramp rate of 50 A/min in 100 A steps. After each step, the current was kept constant for 200 s to wait for the current to settle in the superconducting layers of the non-insulated tapes and thus for the voltage and the magnetic field to reach a constant value. Fig. 12 illustrates the measured voltage over coil I and coil II and the applied current versus time. During powering the coils, the Hall probe was placed perpendicular to the magnetic field generated by the coils and delivered an output voltage that is proportional to the magnitude of the magnetic field. Using a 9th-order polynomial fit the magnetic field was calculated from the measured Hall voltage. Because of placing the whole setup well-immersed in the coolant, all the voltage leads and connections are kept at the same temperature and the thermo-electric voltages are negligible. According to the Hall probe data sheet which was provided by the manufacturer, the overall thickness of the hall sensor is 1.1 mm. Therefore, to compare the measurement with the simulation results, the Opera results were calculated at 0.55 mm distance from the pole tip of the magnet. In Fig. 13, a comparison of the measured and simulated magnetic field versus the applied current reveals a very good agreement, with less than a 1% difference between the experimental and simulated data. These minor discrepancies may stem from simulation errors, like the slight variations in the material B-H curve between the simulated model and the actual sample. These differences may also be attributed to measurement errors, such as minor inaccuracies resulting from power supply fluctuations or the precision limitations of the hall probe.

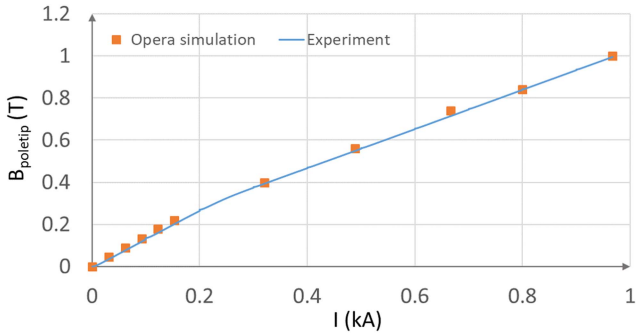

Fig. 13. Magnetic field on pole tip versus applied current, obtained by Hall-probe measurement and Opera simulation at 4.2 K.

Moreover, the voltage decay was approximated using an exponential fit function and the average time constants for coil I and coil II were calculated to be 6 and 6.7 s, respectively. These small time constants of the coils, combined with the magnet's steady-state operation, effectively reduce the potential influence of current redistribution in the NI coils on the field quality. A more thorough examination of this aspect is slated for the next phase of the project.

Also, the investigation into the ohmic heat generated by soldering joints between the coils and the HTS bridges, with a face-to-face joint area resistance of $R_{\mathrm{joint,f2f}} = 36\ \mathrm{n\Omega\ cm^2}$ at 4.2 K [17], indicates that each joint, with an area of 1.44 $\mathrm{cm^2}$ and a current of 0.5 kA, dissipates a total power of 6.25 mW. Considering 8 soldering joints for each one-fourth of a magnet period, the total dissipation power for each period of the quadrupole and the entire magnet structure consisting of 3 periods are 200 mW and 600 mW, respectively. This amount of heat load is estimated to be well cooled by conduction cooling using standard 1 W cryocoolers or if needed larger 1.5 W ones.

VI. Conclusion and Outlook

A novel periodic iron-core quadrupole magnet featuring simple pancake-shaped High-Temperature Superconducting (HTS) coils was designed and successfully implemented in a specific application of a transport line from LPA to the TGU. To validate the design and technical feasibility of the periodic quadrupole magnet, a demonstrator was fabricated which demonstrated promising results. In the experiment, the HTS coils were successfully and stably energized with currents of 150 A and 1000 A, at temperatures of $T = 77$ K and 4.2 K, respectively, showing no degradation. To assess the functional capabilities of the coils in generating the requisite magnetic field, measurements of the pole tip field were conducted using a fixed Hall probe. The acquired measurement results were then compared against the outcomes of calculations, yielding a high level of consistency, less than 1%, between the experimental and simulated data. As the next step, it is planned to further improve the bridge connection, e.g. by adding a copper piece on top, with the goal of powering the magnet using even higher currents in the region of 1.4 kA.

Acknowledgment

The authors would like to acknowledge Mr. Kevin Krauth (Technik-Haus, KIT), Mr. Sascha Westenfelder (ITEP, KIT), and Ms. Nicole Glamann (IBPT, KIT) for their valuable support in manufacturing of the winding body, winding the coils, and preparing the measurement setup.

References

[1] D. A. Jaroszynski et al., "Radiation sources based on laser-plasma interactions," *Philos. Trans. Roy. Soc. A: Math., Phys. Eng. Sci.*, vol. 364, pp. 689–710, 1840, doi: 10.1098/rsta.2005.1732.

[2] W. Wang et al., "Free-electron lasing at 27 nanometres based on a laser wakefield accelerator," *Nature*, vol. 595, pp. 516–520, 2021, doi: 10.1038/s41586-021-03678-x.

[3] J. P. C. Cabadağ et al., "Stable multi-day performance of a laser wakefield accelerator for FEL applications," in *Proc. Free-Elect. Laser*, 2022, pp. 196–200, doi: 10.18429/JACoW-FEL20022-TUP19s41586-021-03678-x.

[4] G. Fuchert, A. Bernhard, S. Ehlers, P. Peiffer, R. Rossmanith, and T. Baumbach, "A novel undulator concept for electron beams with a large energy spread," *Nucl. Instruments Methods Phys. Res. Sect. A: Accelerators, Spectrometers, Detectors Assoc. Equip.*, vol. 672, pp. 33–37, 2012, doi: 10.1016/j.nima.2011.12.097.

[5] C. Widmann, "Simulation and first experimental tests of an electron beam transport system for a laser wakefield accelerator," Ph.D. dissertation, Karlsruhe Inst. Technol., Karlsruhe, Germany, 2015, doi: 10.5445/IR/1000055008.

[6] M. Ning, "A new transport line for transverse gradient undulator experiments at the JETI laser-plasma accelerator in Jena," Master thesis, Karlsruhe Inst. Technol., Karlsruhe, Germany, 2021.

[7] S. Fatehi, A. Bernhard, and A. -S. Müller, "Miniature High strength transport line design for laser plasma accelerator-driven FELs," in *Proc. Int. Part. Accel. Conf.*, 2021, pp. 561–564.

[8] S. Fatehi, "Compact high-temperature superconducting magnets for laser-plasma accelerator beam capture and transport," Ph.D. dissertation, Karlsruhe Inst. Technol., Karlsruhe, Germany, 2023, doi: 10.5445/IR/1000158431.

[9] S. Fatehi, A. Bernhard, and A. -S. Müller, "A short-length transport line for laser-plasma accelerators using HTS periodic magnets," in *Proc. Int. Part. Accel. Conf.*, 2023, Paper 2627, doi: 10.18429/JACoW-IPAC-23-WEODC1.

[10] Dassault Systmès, "CST studio suite (2021) [Software]," 2021. [Online]. Available: https://www.3ds.com/de/produkte-und-services/simulia/produkte/cst-studio-suite

[11] Dassault Systèmes, "[Software] Opera," 2022. [Online]. Available: https://www.3ds.com/de/produkte-und-services/simulia/produkte/opera/

[12] K. Floettmann, "[Software] Astra: A space charge tracking algorithm," Manual, version 3, 2021. [Online]. Available: https://www.desy.de/mpyflo/Astra_manual/Astra-Manual_V3.2.pdf

[13] SuperPower Inc. [Online]. Available: http://www.superpower-inc.com/

[14] S. Hahn, D. K. Park, J. Bascunan, and Y. Iwasa, "HTS pancake coils without turn-to-turn insulation," *IEEE Trans. Appl. Supercond.*, vol. 21, pp. 1592–1595, Jun. 2011, doi: 10.1109/TASC.2010.2093492.

[15] "HTS critical current database," Mar. 2021. [Online]. Available: https://htsdb.wimbush.eu/dataset/4256624

[16] E. Mashkina et al., "Magnetic field test facility for superconductive undulator coils," *IEEE Trans. Appl. Supercond.*, vol. 18, no. 2, pp. 1637–1640, Jun. 2008, doi: 10.1109/TASC.2008.920563.

[17] J. Fleiter and A. Ballarino, "In-field electrical resistance at 4.2 K of REBCO splices," *IEEE Trans. Appl. Supercond.*, vol. 27, no. 4, Jun. 2017, Art. no. 6603305, doi: 10.1109/TASC.2017.2659618.